KSME

Springer

Journal of Mechanical Science and Technology 36 (1) 2022

Original Article
DOI 10.1007/s12206-021-1242-4

Keywords:
· Water-lubricated
· Water injection parameters
· Single-screw air compressor
· Heat transfer

Correspondence to:
Yanan Li
lyn2018@emails.bjut.edu.cn

Citation:
Li, Y., Wang, J., Wu, Y., Lei, B., Zhi, R., Shen, L. (2022). Influence of water injection parameters on the performance of a water-lubricated single-screw air compressor. Journal of Mechanical Science and Technology 36 (1) (2022) 445~456. http://doi.org/10.1007/s12206-021-1242-4

Received April 13th, 2021
Revised July 4th, 2021
Accepted October 4th, 2021

† Recommended by Editor Tong Seop Kim

Influence of water injection parameters on the performance of a water-lubricated single-screw air compressor

Yanan Li[1,2], Jingfu Wang[1,2], Yuting Wu[1,2], Biao Lei[1,2], Ruiping Zhi[1,2] and Lili Shen[1,2]

[1]Faculty of Environment and Life, Beijing University of Technology, Beijing 100124, China, [2]Key Laboratory of Enhanced Heat Transfer and Energy Conservation, Beijing University of Technology, Beijing 100124, China

Abstract A thermodynamic model of a water-lubricated single-screw air compressor was established to examine the impact of water injection parameters on performance. Heat transfer and leakage between humid air and water was considered by analyzing the impacts of rotation speed, discharge pressure, the rate of water injection, and diameter of droplets on the performance of a compressor. The discharge temperature could be reduced by increasing the rate of water injection, resulting in the compression procedure moving towards an isothermal state. The increase in the rate of water injection under rated conditions from 60 L/min to 80 L/min resulted in a reduction in the compressor discharge temperature, increased the volume efficiency, and increased adiabatic efficiency by 11.1 K, 1.5 %, and 2.8 %, respectively. Water injection atomization increased the area of transfer of heat between humid air and water and improved the performance of compressor.

1. Introduction

There has recently been increasing importance placed on food and medicine safety, production quality control within the textile, precision electronics, and other industries, and the production of hydrogen fuel cells to power vehicles. These developments have seen increasingly pressing need for improved compressed air quality, in particular clean air that is free from oil. Achieving the production of completely oil-free compressed air is a challenge that urgently requires a solution within the compressor industry. Water-lubricated air compressors use pure water as a lubrication medium, thereby avoiding pollution of compressed air. In addition, the pure water injected into the compression chamber can play a role in cooling, sealing, and noise reduction. Therefore, the state of the compression procedure in water-lubricated air compressors is close to isothermal, thereby reducing the energy consumption of the machine. Hence, water-lubricated air compressors provide an effective and feasible approach to achieving oil-free compressed air.

There have been many past studies on water-lubricated compressors. Zhao et al. developed a thermodynamic theoretical model of the water-lubricated scroll compressor for automotive fuel cell systems that considered the impact of heat transfer and leakage, which they used to analyze the impact of the rate of water injection on the compressor' thermal performance [1]. Li et al. developed a theoretical model of the water-injected twin-screw air compressor and conducted experiments to test that the performance of the compressor gradually increases with increasing water injection flow rate [2]. Shen et al. examined the water-injected twin-screw compressor applied to the single-impact mechanical vapor compression desalination system and compared the temperature of discharge and consumption of power under conditions of water injection and no water injection. The discharge temperature and consumption of power of a compressor can be reduced through the injection of water [3]. Wang et al. conducted experiments to study the impacts of discharge pressure, water flow rate, rotation speed and water injected position on the water- lubricated twin-screw air compressor performance [4]. Subse-

quently, a model of the water-lubricated twin-screw air compressor, including a heat transfer and detailed leakage model, was proposed to analyze its leakage [5]. Tian et al. studied the application of the water vapor twin-screw compressor in mechanical vapor compression heat pump systems in which the transfer of mass and heat between liquid water and water vapor was considered, with the results verifying that water injection improved the performance of the compressor [6].

The above studies on water-lubricated compressors mainly focused on scroll and twin-screw compressors. In recent years, single screw water-lubricated compressors have overcome the triangle leakage area problem suffered by the twin screw structure, and the axial and radial force of air carried by the screw can be automatically balanced. This development has the advantages of balanced force, reduced vibration, reduced noise, an extended service life, increased efficiency, and wide range of applicable pressures. Therefore, the water-lubricated single screw air compressor (WLSSAC) has gradually become the preferred choice to provide oil-free compressed air.

There have been many past studies on the single-screw compressor. Wang et al. conducted a detailed research on the geometric characteristics of the working chamber's inner surface, heat transfer characteristics, and leakage of the multicolumn envelope meshing pair single-screw refrigeration compressor [7-9]. Wen et al. proposed a novel approach to calculate the area of the injection aperture of the single-screw refrigeration compressor, established a thermodynamic model representing the compressor, including the injection procedure, and experimentally verified that the injection could decrease the compressor's discharge temperature [10]. Lu et al. researched the performance of the single-screw refrigeration compressor with different meshing clearance [11].

However, the aforementioned studies mainly concerned with the oil-injected single-screw compressor. The viscosity, specific heat, and other parameters of water differ from those of oil; therefore, establishing a theoretical calculation model for the operating procedure of a WLSSAC is necessary to analyze the impact of water injection parameters on its performance.

Studies on WLSSAC performance remain limited. Li et al. examined the impacts of different meshing pair lines on a single-screw compressor's hydrodynamic lubrication parameters using both theoretical and experimental approaches and determined that an optimal impact of water lubrication can be obtained using the multiple cylindrical meshing pair [12-15]. Yet, there has to date been no study on the impact of water injected parameters on compressor performance. Yang et al., in a study of a system of mechanical vapor recompression using a water-injected single-screw compressor and the impact of rate of water injection on compressor performance, showed that the performance of a vapor compressor could be enhanced by atomization of water injection [16]. Despite the similarity of the mechanical structures of vapor compressors and air compressors, their working conditions and thermal performance differ considerably.

Therefore, the present study focused on a WLSSAC. It is important to consider the water injection parameters within the design of a WLSSAC as they directly affect the performance of the compressor. Therefore, the current study developed a thermodynamic model representing a WLSSAC to study the impacts of rotation speed, discharge pressure, water injection flow rate, and diameter of droplets on the compressor performance. The results of the current research can act as a reference frame for the design and optimization of a WLSSAC.

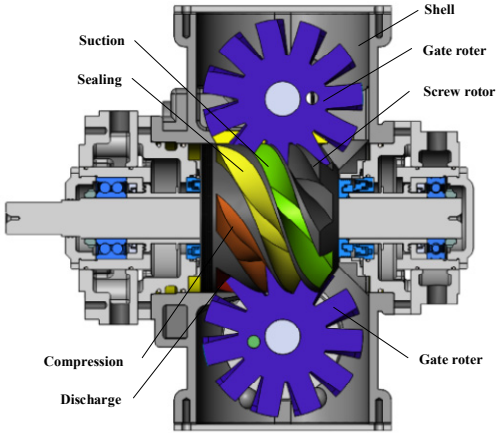

Fig. 1. An illustration of the WLSSAC's operating procedure.

2. Model of a WLSSAC

As illustrated in Fig. 1, the main components of a WLSSAC include a gate rotor, a screw rotor, and shell. The teeth number to screw rotor ratio of the gate rotor is 6/11. The screw is rotated by the motor drive, with the change in the screw angle altering the volume of the working chamber.

2.1 Assumptions

The operating procedure of a WLSSAC is complex. There are three forms of working medium: (1) water; (2) water vapor, and; (3) dry air. The establishment of the mathematical model of the operating procedure was made under the following assumptions to simplify the calculation:

1) Kinetic energy and potential changes of fluids were ignored.

2) Uniform distributions of pressure and temperature were assumed in different fluid in the control volume. In addition, there were periodic changes to the working medium's state parameters in response to changes to the screw rotation angle.

3) The density of water remained constant.

4) Water vapor remained in a state of saturation.

5) Pressure pulsation during the procedure of suction was ignored.

6) Water exists in a two states, namely liquid droplets and liquid film, with the latter evenly attached to the wall surface of controlled volume, and the transfer of heat between the liquid film and the wall surface was neglected.

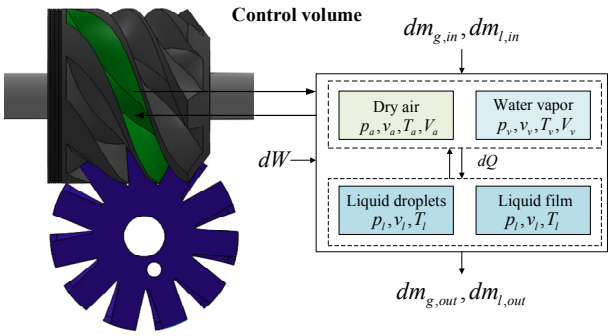

Fig. 2. The control volume of a WLSSAC.

7) There was a constant ratio of the mass of droplets to water total mass in the control volume, defined as the atomization ratio.

2.2 Governing equations

As shown in Fig. 2, of all the working screw groves, the present study selected one as the control volume.

The gas phase in the control volume comprises uniformly mixed dry air and saturated steam, resulting in their equal temperatures and the sum of the partial pressures being equal to that of humid air. The liquid phase in the screw groove exists in two forms, namely droplets and film, and its pressure is equal to that of humid air. Given the large volume of water injected into the screw groove, the volume of the groove occupied by water cannot be ignored. In conclusion, the following equation can be obtained:

$$\begin{cases} T_g = T_v = T_a \\ p_l = p_g = p_a + p_v \\ V_g = V_v = V_a \\ V_c = V_g + V_l \end{cases}. \tag{1}$$

In Eq. (1), χ is the fraction of the mass of the gas in the control volume. Given Eq. (1), the variations in each component's mass with the angle of screw rotation is:

$$\begin{cases} \dfrac{dm}{d\theta} = \dfrac{dm_g}{d\theta} + \dfrac{dm_l}{d\theta} \\ \dfrac{dm_l}{d\theta} = (1-\chi)\dfrac{dm}{d\theta} = \dfrac{1-\chi}{\chi}\dfrac{dm_g}{d\theta} \\ \dfrac{dm_a}{d\theta} = \dfrac{1}{1+d}\dfrac{dm_g}{d\theta} \end{cases}. \tag{2}$$

The differential equation defining internal energy and mass of each component with a change in the angle of rotation of the screw can be obtained according to the conservation of energy and mass. Here, the equation defining the conservation of mass of humid air is:

$$\frac{dm_g}{d\theta} = \frac{dm_{g,in}}{d\theta} - \frac{dm_{g,out}}{d\theta}. \tag{3}$$

The equation defining the mass conservation of water is:

$$\frac{dm_l}{d\theta} = \frac{dm_{l,in}}{d\theta} - \frac{dm_{l,out}}{d\theta}. \tag{4}$$

The equation defining the mass conservation of water vapor is:

$$\frac{dm_v}{d\theta} = \frac{dm_{v,in}}{d\theta} - \frac{dm_{v,out}}{d\theta} + \frac{dm_e}{d\theta}. \tag{5}$$

The equation defining the energy conservation of dry air is:

$$\frac{d(m_a u_a)}{\mathrm{d}\theta} = \sum \frac{dm_{a,in}}{\mathrm{d}\theta} h_{a,in} - \sum \frac{dm_{a,out}}{\mathrm{d}\theta} h_{a,out} - \frac{dQ_a}{\mathrm{d}\theta} - p_a \frac{dV_a}{d\theta}. \tag{6}$$

The equation defining the conservation of energy of water is:

$$\frac{d(m_l u_l)}{\mathrm{d}\theta} = \sum \frac{dm_{l,in}}{\mathrm{d}\theta} h_{l,in} - \sum \frac{dm_{l,out}}{\mathrm{d}\theta} h_{l,out} - \frac{dQ_l}{\mathrm{d}\theta}. \tag{7}$$

The basic thermodynamic equations as shown were used:

$$\begin{cases} h = u + pv \\ u_l = c_l T_l \\ v = V / m \\ dW = pdV \end{cases}. \tag{8}$$

The differential equations of the pressure and specific volume of dry air and the temperature of water in the controlled volume with changes to screw rotation are obtained as follows:

$$\frac{dp_a}{\mathrm{d}\theta} = \frac{1}{1 - \dfrac{1}{v_a}\dfrac{(\partial h_a / \partial T_a)_v}{(\partial p_a / \partial T_a)_v}} \left(\begin{array}{l} \dfrac{1}{v_a}\left[(\dfrac{\partial h_a}{\partial v_a})_T - \dfrac{\left(\dfrac{\partial h_a}{\partial T_a}\right)_v \left(\dfrac{\partial p_a}{\partial v_a}\right)_T}{(\partial p_a / \partial T_a)_v} \right] \dfrac{dv_a}{d\theta} \\ -\dfrac{1}{V_a}\left[\sum \dfrac{dm_{a,in}}{d\theta}(h_{a,in} - h_a) - \dfrac{dQ_a}{d\theta} \right] \end{array} \right), \tag{9}$$

$$\frac{dv_a}{d\theta} = \frac{1}{m_a}\frac{dV_a}{d\theta} - \frac{V_a}{m_a^2}\frac{dm_a}{d\theta}, \tag{10}$$

$$\frac{dT_l}{\mathrm{d}\theta} = \frac{1}{m_l}\left(\sum \frac{dm_{l,in}}{\mathrm{d}\theta} T_{l,in} - \sum \frac{dm_{l,out}}{\mathrm{d}\theta} T_{l,out} - T_l \frac{dm_l}{\mathrm{d}\theta} + \frac{1}{c_l}\frac{dQ_l}{\mathrm{d}\theta} \right). \tag{11}$$

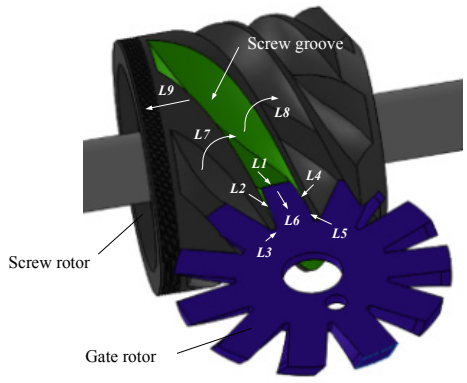

Fig. 3. Leakage channels of single-screw compressor.

2.3 Leakage model

As illustrated in Fig. 3, nine leakage paths exist in the single-screw air compressor. The specific description can be seen in Ref. [17], which will not be repeated here.

When water is injected into the working chamber the working medium changes into a water-gas two-phase fluid. In the current study, the passage of fluid along each leakage path was regarded as two-phase laminar flow. The mass fraction of the leakage channel gas was assumed to equal that of the gas in the working chamber. According to the leakage model in Refs. [17, 18], the leakage model of a WLSSAC is given as:

$$\begin{cases} \dfrac{dm_g}{d\theta} = C_{lea}\alpha S\rho_g v_g / \omega \\ \dfrac{dm_l}{d\theta} = C_{lea}(1-\alpha)S\rho_l v_l / \omega \\ v_g = \sqrt{2(h_l - h_2)} \\ v_l = v_g / f \\ f = 0.4 + 0.6\sqrt{\dfrac{\rho_l}{\rho_g} + 0.4\left(\dfrac{1}{\chi} - 1\right)}\sqrt{1 + 0.4\left(\dfrac{1}{\chi} - 1\right)} \\ \alpha = \dfrac{1}{1 + f\left(\dfrac{1}{\chi} - 1\right)\dfrac{\rho_g}{\rho_l}} \end{cases} . \quad (12)$$

In Eq. (12), h_1 is the enthalpies of the high-pressure chamber; h_2 is the enthalpies of the high-pressure chamber.

2.4 Heat transfer model

Since a large volume of water is injected into the WLSSAC, the heat transfer between water and gas cannot be ignored. Besides, there is a gradual rise in water temperature due to the large specific heat capacity of water. Therefore, it cannot be assumed that the temperature of water is equal to that of air. It was assumed in the current study that the injected water in the compressor was present in two forms, namely film and droplets. Film attached uniformly to the surface of the control volume. Hence, the total transfer of heat between humid air and water is equal to the transfer of convective heat between droplets and humid air plus that between liquid film and humid air:

$$\frac{dQ}{d\theta} = \frac{dQ_{film}}{d\theta} + \frac{dQ_{drop}}{d\theta} . \quad (13)$$

Meanwhile, the transfer of heat between humid air and water leads to two outcomes. On the one hand, sensible heat transfer increases water temperature, whereas on the other, latent heat transfer results in the evaporation of water into water vapor, then:

$$\frac{dQ}{d\theta} = \frac{dQ_l}{d\theta} + \frac{dQ_e}{d\theta} . \quad (14)$$

The following can be obtained from Eqs. (13) and (14):

$$\frac{dQ_l}{d\theta} = \frac{dQ_{film}}{d\theta} + \frac{dQ_{drop}}{d\theta} - \frac{dQ_e}{d\theta} . \quad (15)$$

Here, the heat transfer resulting from the evaporation of water varies with the screw rotation angle:

$$\frac{dQ_e}{d\theta} = \frac{dm_e}{d\theta} \cdot r_l . \quad (16)$$

By combining with Eq. (5), the mass of evaporated water vapor varies with the screw rotation angle as follows:

$$\frac{dm_e}{d\theta} = \frac{dm_v}{d\theta} - \frac{dm_{v,in}}{d\theta} + \frac{dm_{v,out}}{d\theta} . \quad (17)$$

The change in the transfer of heat between water and dry air with screw rotation is then:

$$\frac{dQ_a}{d\theta} = \frac{dQ}{d\theta} \cdot \frac{c_{pa}}{c_{pa} + dc_{pv}} . \quad (18)$$

A wall temperature was given in the past when calculating the transfer of heat between the working medium and the wall of the control volume [19]. However, the current study adopted the calculation model in the Ref. [5] based on the characteristics of a WLSSAC. It was considered that liquid film uniformly covered the control volume and that the temperatures of the liquid film and the wall were similar. This results in the transfer of heat between humid air and the casing being similar to that between liquid film and humid air. The temperature of the liquid film can be determined by Eq. (7).

The formula defining the transfer of heat by forced convection can be applied to determine the transfer of heat between humid air and water. The coefficient of the transfer of heat can be identified by the approach used by *Nu* [20]. Here, the change in heat transfer between liquid film and humid air re-

sulting from screw rotation angle can be calculated as [21, 22]:

$$\begin{cases} \dfrac{dQ_{film}}{d\theta} = k_{film} S_{film} \left(T_g - T_l\right) / \omega \\ k_{film} = Nu_{film} \lambda_g / d_e \\ Nu_{film} = 0.023 Re_{film}^{0.8} Pr_{film}^{0.3} c_r \\ Re_{film} = \rho_g v_{g,film} d_e / \mu_g \\ v_{g,film} = \left| \dfrac{1}{S_{end}} \dfrac{\partial V_c}{\partial t} \right| \\ c_r = 1 + 1.77 \times 2 d_e / \left(r_o + r_i\right) \\ d_e = r_2 - a / \cos\theta_2 \end{cases} . \tag{19}$$

In Eq. (19), S_{film} is the wall area of the control volume, and since the procedure of gas flow in the groove is complicated, the groove is equivalent to the spiral tube, $v_{g,film}$ is the velocity of the humid air relative to the liquid film, S_{end} is the area of the gate rotor into the screw groove, $\partial V_c / \partial t$ is the rate of change of the volume of the screw groove, and d_e is the equivalent diameter of the gate rotor feeding the screw groove.

The transfer of heat between droplets and humid air in response to changes in the rotation angle of the screw can be obtained by [23]:

$$\begin{cases} \dfrac{dQ_{drop}}{d\theta} = k_{drop} S_{drop} \left(T_g - T_l\right) / \omega \\ k_{drop} = Nu_{drop} \lambda_g / d_{drop} \\ Nu_{drop} = 2 + 0.6 Re_{drop}^{0.5} Pr_{drop}^{0.33} \\ Re_{drop} = \rho_g v_{g,drop} d_{drop} / \mu_g \\ v_{g,drop} = \left| \vec{v}_{drop} - \vec{v}_g \right| \\ S_{drop} = \pi d_{drop}^2 \dfrac{\zeta m_l}{\frac{1}{6} \rho_l \pi d_{drop}^3} = \dfrac{6 \zeta m_l}{\rho_l d_{drop}} \end{cases} . \tag{20}$$

The law regulating the motion of water injected into the screw groove is complicated, and the calculation can be simplified by introducing the atomization rate ζ, which equals the percentage of mass of droplets making up the total water mass. The value of the atomization rate is 1 when all water is in a droplet form. During the operation of the compressor, it is not possible for all the water injected into the compressor to float in the screw groove in the form of water droplets, resulting in its value ranging between 0 and 1.

With the injection of water into the operating chamber, the direction of droplet velocity is perpendicular to the screw axis, and the magnitude of velocity is the ratio between the volume rate of the water injected and the area of the water injection aperture:

$$v_{drop} = q_{v,inj} / S_{inj} . \tag{21}$$

The speed of axial movement of the gas along the screw can be written as:

$$v_g = \omega r_1 \frac{L_s}{2\pi r_1 \frac{\theta_{eng}}{2\pi}} = \frac{\omega L_s}{\theta_{eng}} . \tag{22}$$

2.5 Water-injection model

The Bernoulli equation representing from the inlet section of the water injection aperture to the outlet section is:

$$\frac{v_1^2}{2g} + z_1 + \beta_1 \frac{p_1}{\rho_l g} = \frac{v_2^2}{2g} + z_2 + \beta_2 \frac{p_2}{\rho_l g} . \tag{23}$$

The inlet velocity is approximately 0, and by ignoring the change in position, the outlet section velocity can be obtained as:

$$v_2 = C_{inj} \sqrt{2\left(p_1 - p_2\right) / \rho_l} . \tag{24}$$

Then, the water injected mass flow rate is:

$$\frac{dm_{inj}}{dt} = C_{inj} S_{inj} \rho_l \sqrt{2\left(p_1 - p_2\right) / \rho_l} . \tag{25}$$

In Eq. (25), v_1 and v_2 are the velocities of water at the inlet and outlet of the water injection aperture, respectively, whereas p_1 and p_2 are the pressures of water at the inlet and outlet of the water injection aperture, respectively.

2.6 Performance parameters

The volume efficiency is an important parameter to evaluate the performance of a compressor and indicates the optimal utilization of the geometry size of a compressor and assesses the impact of leakage on the performance of the compressor. Volume efficiency can be calculated as follows:

$$\eta_v = q_{v,real} / q_{v,th} . \tag{26}$$

The theoretical volume flow rate is:

$$q_{v,th} = 2 n z_1 V_{in} . \tag{27}$$

The actual mass flow in the calculation model is:

$$\dot{m}_{real} = \dot{m}_{th} - \dot{m}_{lea} . \tag{28}$$

The following equation defining the adiabatic efficiency of compressor:

Table 1. Operating parameters and main structure of the WLSSAC.

Parameters	Value
Screw rotor's diameter	147 mm
Gate rotor's diameter	158 mm
Center distance	117.6 mm
Gate rotor tooth width	21.9 mm
Rotation speed	3000 rpm
Rated power	11 KW
Internal volume ratio	3
Rotor length	120.55 mm
Theoretical flowing capacity	200 m^3/h
Suction pressure	0.1013 MPa
Suction temperature	298.15 K
Temperature of injected water	298.15 K

$$\eta_{ad} = P_{ad} / P_s . \tag{29}$$

The following equation defining the power of adiabatic compression:

$$P_{ad} = \dot{m}_{real} \left(h_{d,ad} - h_{in} \right) . \tag{30}$$

The equation for determining the power consumed by compressed humid air is:

$$P_{s,g} = \dot{m}_{real} \int_{p_i}^{p_d} -v dp . \tag{31}$$

Power consumption by compressed water is:

$$P_{s,l} = \dot{m}_l \left(p_d - p_{in} \right) / \rho_l . \tag{32}$$

The consumption of power by the compressor is:

$$P_s = P_{s,g} + P_{s,l} . \tag{33}$$

The compressor specific power equals the gas flow consumed power per unit volume. The calculation equation is as follows:

$$P_{sp} = P_s / q_{v,real} . \tag{34}$$

2.7 Simulation parameters

The operating and main structure parameters of the compressor in the simulation are listed in Table 1.

3. Results and discussion

3.1 Impact of rotation speed and discharge pressure

Fig. 4 shows the impact of the rotation speed and discharge pressure on the water-gas volume ratio and volume efficiency of a WLSSAC. As displayed in Fig. 4(a), volume efficiency increased with improving rotation speed at a fixed discharge pressure. A rise in the rotation speed from 1500 rpm to 3000 rpm caused an increase in volume efficiency of 12.6 % from 67.1 % to 79.7 % at the rated discharge pressure of 0.467 MPa. This consequence could be credited to the relationship between volume efficiency and leakage quantity. The rate of leakage of a single operating screw groove was largely fixed under varying rotation speeds, with the duration and quantity of leakage inversely related to the rotation speed. In addition, as illustrated in Fig. 4(b), the screw groove water-gas ratio declined with increasing rotation speed, which impacted the impacts of transfer of heat and sealing, resulting in an increase in leakage. Hence, the rise in the volume efficiency rate decreased with rising rotation speed.

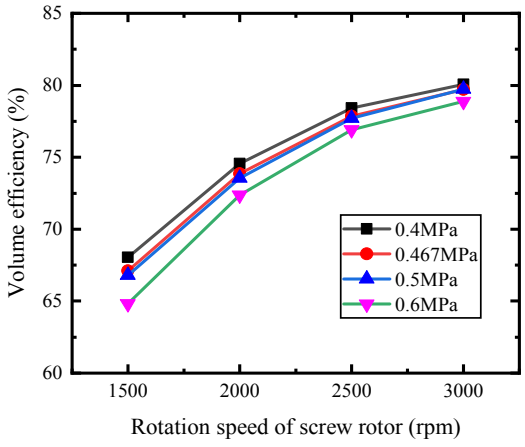

(a) Volume efficiency

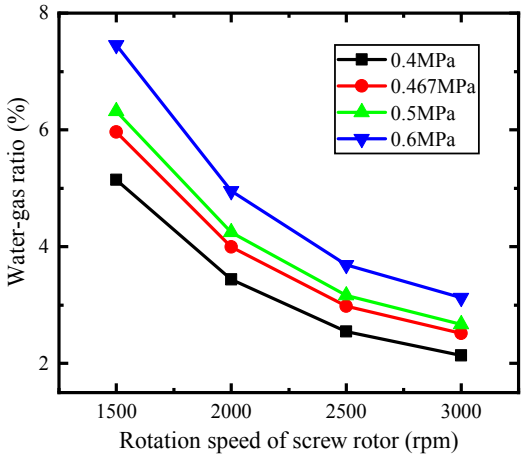

(b) Water-gas volume ratio

Fig. 4. Impact of the rotation speed and discharge pressure on the water-gas volume ratio and volume efficiency of a WLSSAC.

The increase in discharge pressure had two impacts under a constant rotation speed. On the one hand, there was an increase in the difference in pressure between the working chamber and the leakage chamber, resulting in an increase in

leakage. On the other hand, there was an increase in the pressure difference before and after the water injection aperture. In addition, as displayed in Fig. 4(b), there were increases in water injected into the working volume and in the screw groove water-gas volume ratio, which reduced leakage. The former played a dominant role at low rotation speeds, with a clear reduction in volume efficiency with the increment in discharge pressure. In contrast, at a high speed, the latter played an important role, resulting in a slight reduction in volume efficiency due to increasing discharge pressure. For example, at rotation speeds 1500 rpm and 3000 rpm and an increase in discharge pressure from 0.4 MPa to 0.6 MPa resulted in decline the volume efficiency of 3.3 % and 1.2 %, respectively.

As shown in Fig. 4(b), under a constant discharge pressure, there was a decline in the rate of injected water but an increase in the rate of flow of gas with an increment in rotation speed, resulting in a decline in the water-gas ratio. However, the rise in the rate of gas volume flow gradually slowed with an increment in rotation speed above 3000 rpm, with the curve gradually plateauing.

An increase in discharge pressure under a fixed rotation speed resulted in a rise in the rate of injected water and a decline in the gas flow rate, further leading to an increase in the water-gas volume ratio. The decrease in the gas flow rate at a low rotation speed with increasing discharge pressure surpassed that at a high rotation speed. At a high rotation speed, there was a gradual slowing in the decrease in the rate of gas flow resulting from the increase in discharge pressure, resulting in a relatively small increase in the water-gas volume ratio due to a rise in discharge pressure. An increase in the discharge pressure from 0.4 MPa to 0.6 MPa resulted in improve the water-gas volume ratio of 2.3 % at 1500 rpm and 1 % at 3000 rpm.

As shown in Fig. 5, there was a gradual rise in adiabatic efficiency with raising rotation speed. However, the rate of increase slowed gradually, which could be ascribed to adiabatic efficiency representing the ratio of adiabatic compression work to actual work consumption. Leakage decreased with a rise in rotation speed, lead to a decrease in leakage consumption of power. Meanwhile, there was a decline in the performance of heat transfer and an increment in consumption of power with the water-gas volume ratio reduced. Under a pressure of discharge of 0.4 MPa, the impact of the latter exceeded that of the former when the rotation speed increased to 2500 rpm due to the existence of over compression, causing a decline in the adiabatic efficiency.

As shown in Fig. 6, there was a gradual decrease in specific power with rising rotation speed at a fixed discharge pressure. A rise in the rotation speed from 1500 rpm to 3000 rpm at the rated discharge pressure resulted in a decrease in the specific power by 0.59 kW/(m^3/min). The rate at which specific power declined with rising rotation speed gradually slowed because the specific power is the ratio between actual consumption of power and actual discharge capacity. The above analysis showed that the rate at which specific power decreased slowed

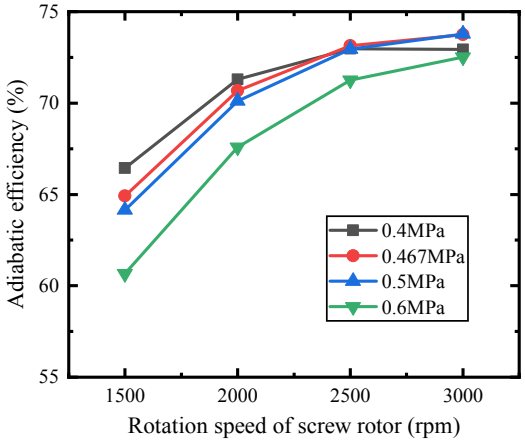

Fig. 5. Impact of rotation speed and discharge pressure on adiabatic efficiency of a WLSSAC.

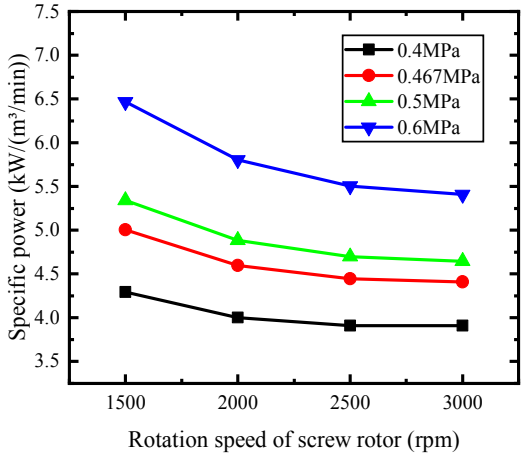

Fig. 6. Impact of rotation speed and discharge pressure on adiabatic efficiency of a WLSSAC.

as the rate of increase in volume efficiency gradually slowed. It was also clear that at each discharge pressure, there was a small difference in specific power between rotation speeds of 3000 rpm and 2500 rpm, indicating that specific power cannot be improved by continuing to increase rotation speed. Under a constant rotation speed, there was a gradual decrease in specific power with decreasing discharge pressure. When the discharge pressure was reduced from 0.6 MPa to 0.4 MPa, the specific power was reduced to 1.49 kW/(m^3/min) at 3000 rpm.

3.2 Impact of rotation speed and water injection flow rate

As shown in Fig. 7, discharge temperature decreased from 320.6 K to 309.5 K with a rise in the rate of water injection at the rated rotation speed. This means that injected water reduces the temperature of discharge of a single-screw air compressor.

Fig. 8 shows the impact of the rate of water injection on the p-V diagram. As displayed in Fig. 8, the curve gradually transi-

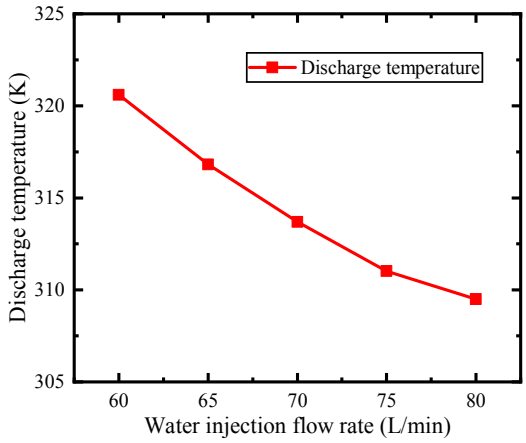

Fig. 7. Impact of water injection flow rate on temperature of discharge of a WLSSAC.

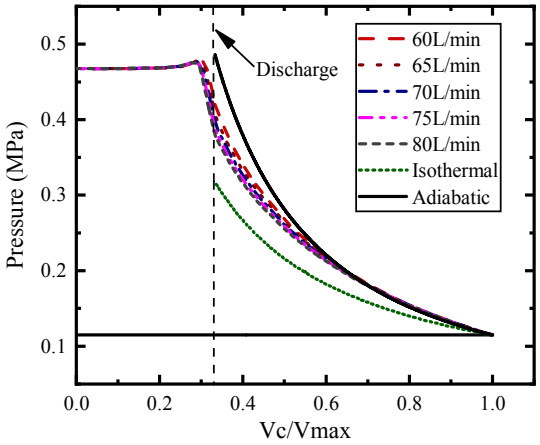

Fig. 8. Impact of water injection flow rate on the p-V diagram of a WLSSAC.

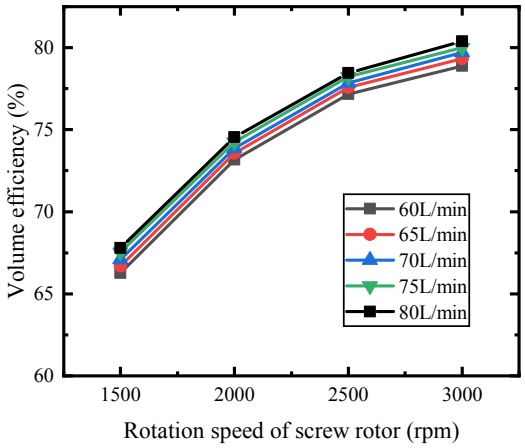

(a) Volume efficiency

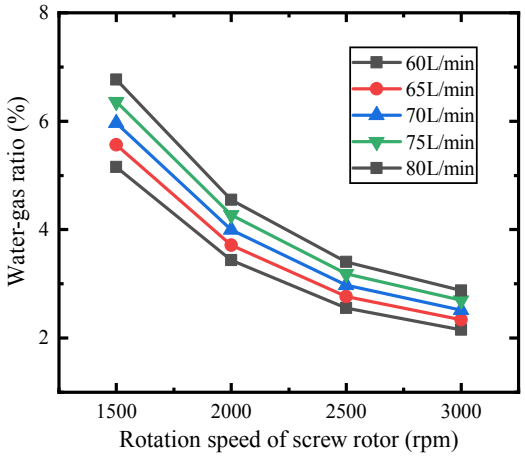

(b) Water-gas volume ratio

Fig. 9. Impact of the rotation speed and rate of water injection on the water-gas volume ratio and volume efficiency of a WLSSAC.

tioned from adiabatic compression to isothermal compression with an increasing rate of water injection. This is because the transfer of heat between humid air and water increased with increasing rate of water injection, resulting in an improvement in the cooling impact.

Exhibited in Fig. 9(a), volume efficiency increased with rising rotation speed under a fixed rate of water injection. Under a rate of water injection of 80 L/min, the volume efficiency increased by 12.6 % with a rise in the rotation speed from 1500 rpm to 3000 rpm. However, the increased rate of volume efficiency with increasing rotation speed gradually slowed. As with the previous analysis, this was because the increase in rotation speed reduced leakage, and at the same time, reduced the water-gas volume ratio, which affected heat transfer and the sealing impact, further increasing leakage. The latter gradually played a dominant role with increasing rotation speed, resulting in a gradual slowing of the rate of rise in volume efficiency.

At a fixed rotation speed, with increasing the rate of water injection, the compressor was more conducive to clearance sealing and showed a greater ability to reduce leakage, increase the transfer of heat between humid air and water, and reduce the temperature of compressed air, resulting in increased volume efficiency. The maximum volume efficiency of 80.4 % was obtained at the rated rotation speed under a rate of water injection of 80 L/min.

As shown in Fig. 9(b), under a fixed rate of water injection flow, the water-gas volume ratio decreased with increasing rotation speed, although the rate of decrease slowed gradually. Under a constant rotation speed, the water-gas volume ratio increased with an increasing flow rate of water injection. The water-gas ratio ranged between 2.1 %-2.9 % at the rated rotation speed when the rate of water injection raised from 60 L/min to 80 L/min, exceeding that of an oil-injected compressor.

Fig. 10 shows the impact of rotation speed and rate of water injection on adiabatic efficiency, where it is clear that at a fixed rate of water injection, adiabatic efficiency gradually improved with rising rotation speed, with the rate of increase gradually slowing. Hence, the impact of raising rotation speed on the

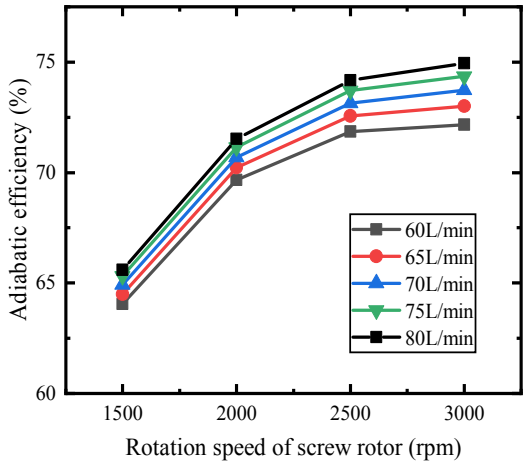

Fig. 10. Impact of the rotation speed and rate of water injection on adiabatic efficiency of a WLSSAC.

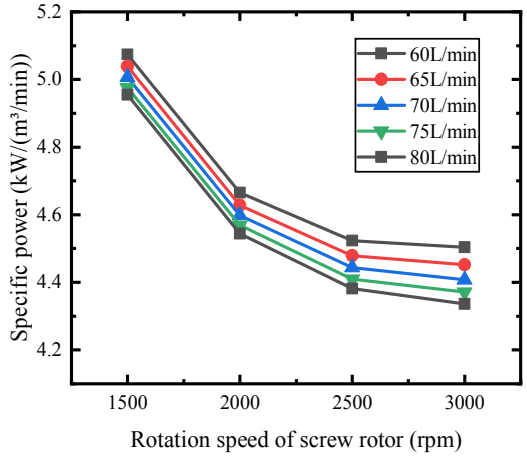

Fig. 11. Impact of the rotation speed and rate of water injection on the specific power of a WLSSAC.

compressor adiabatic efficiency was weakened gradually.

At a fixed rotation speed, adiabatic efficiency increased with increasing rate of water injection. This result could be ascribed to the increment in the rate of water injection improving cooling and sealing, thereby reducing consumption of power. Moreover, the impact of rate of water injection on adiabatic efficiency became increasingly evident with rising rotation speed. An increase in the rate of water injection from 60 L/min to 80 L/min contributed to improvements in adiabatic efficiency of 2.8 % at 3000 rpm and 1.5 % at 1500 rpm.

Fig. 11 shows the impact of rotation speed and the rate of water injection on specific power. At a fixed rate of water injection, there was a gradual decrease in specific power with increasing rotation speed, but the rate of decrease gradually slowing. As shown in Fig. 11, there were only small differences among the curves between rotation speeds of 3000 rpm and 2500 rpm. At a rate of water injection of 80 L/min, there was a decrease in the specific power from 4.9 kW/(m^3/min) to 4.3 kW/(m^3/min) with increasing rotation speed.

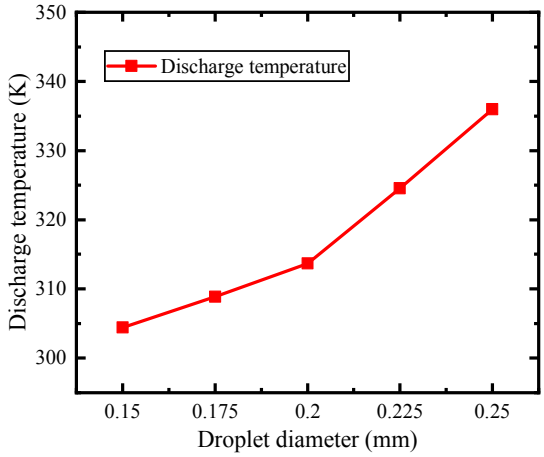

Fig. 12. Impact of the diameter of droplets on temperature of discharge of a WLSSAC.

At a fixed rotation speed, there was an increase in heat transfer with increasing the rate of water injection, which reduced the consumption of power of compressed gas. At the same time, this resulted in an increase in the consumption of power by compressed water. However, since the power consumed by the latter was significantly less than that by the former, the specific power gradually decreased. At a high rotation speed, there was a clear reduction in specific power since there was a greater reduction in consumption of power compared to that under a low rotation speed and under the same increase in the rate of water injection.

At practical application, the rate of water injection can be adjusted by controlling the opening of the inlet valve.

3.3 Impact of the diameters of droplets and rotation speed

Under a fixed rate of water injection, the area of heat transfer could be decreased by increment in atomized droplet diameter, lead to a drop in transfer of heat. As illustrated in Fig. 12, a rise the diameter of droplets from 0.15 mm to 0.25 mm produced a rise the temperature of discharge from 304 K to 336 K under a rate of water injection of 70 L/min and a rated working condition.

As displayed in Fig. 13(a), under a fixed diameter of droplets, volume efficiency increased with rising rotation speed. The volume efficiency increased 12.6 % with increasing rotation speed under a diameter of droplets of 0.2 mm, but the increasing rate slowed gradually.

At a fixed rotation speed, given that a little diameter of droplets improved the transfer of heat and decelerated the screw groove pressure rise, the leakage rate and volume efficiency decreased and increased, respectively. The maximum volume efficiency was obtained at a diameter of droplets and rotation speed of 0.15 mm and 3000 rpm, respectively. The impact of the decrease in the diameter of droplets on volume efficiency was increasingly clear with improve rotation speed.

As displayed in Fig. 13(b), at a fixed rate of water injection,

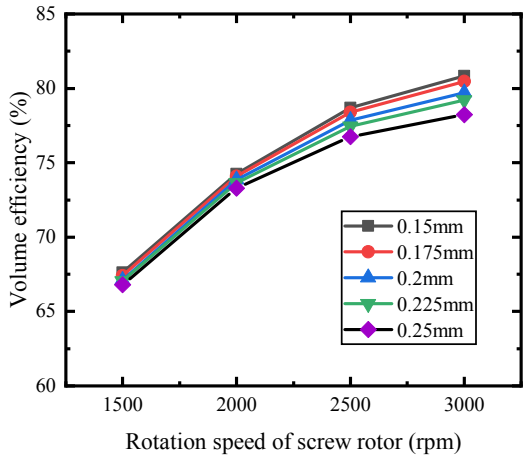

(a) Volume efficiency

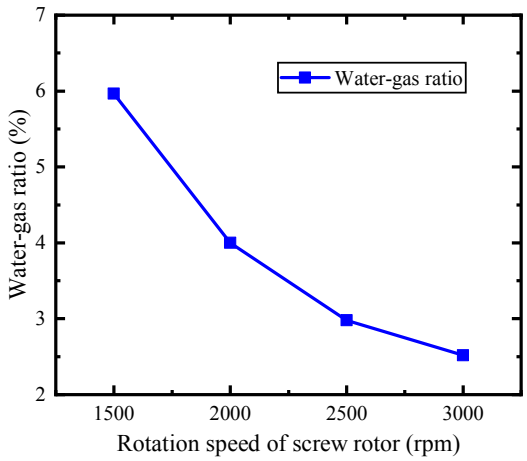

(b) Water-gas volume ratio

Fig. 13. Impact of the diameter of droplets and rotation speed on the water-gas volume ratio and volume efficiency of a WLSSAC.

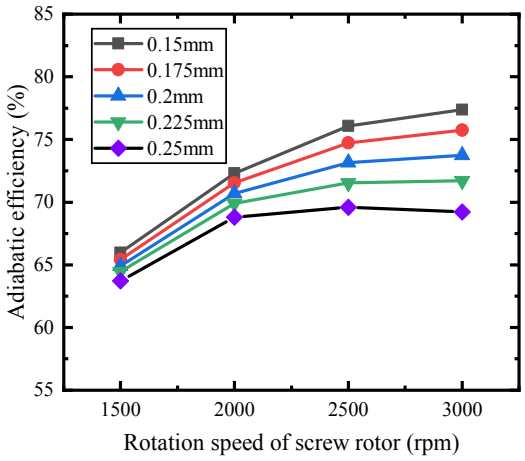

Fig. 14. Impact of the rotation speed and diameter of droplets on adiabatic efficiency of a WLSSAC.

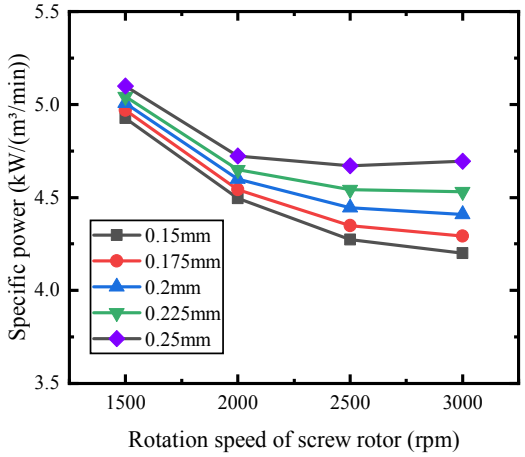

Fig. 15. Impact of rotation speed and diameter of droplets on the specific power of a WLSSAC.

there was only a relationship between the water-gas volume ratio and the rotation speed.

As displayed in Fig. 14, under a diameter of droplets of 0.25 mm, adiabatic efficiency showed an initial increase and then a decline. This outcome could be ascribed to a rise in volume efficiency with rising rotation speed. Meanwhile, a decline in the water-gas volume ratio resulted in an increase in consumption of power. After the rotation speed exceeded a certain threshold, the impact of the rise in consumption of power was higher than that resulting from the rise in volume efficiency. This resulted in a decrease in adiabatic efficiency. Under a fixed diameter of droplets, there was a rise in adiabatic efficiency with rising rotation speed increased to a maximum, with adiabatic efficiency decreasing subsequently.

At a fixed rotation speed, adiabatic efficiency improved with declining diameter of droplets. The highest adiabatic efficiency of 77.4 % was observed at a diameter of droplets and rotation speed of 0.15 mm and 3000 rpm, respectively.

As displayed in Fig. 15, at a diameter of droplets of 0.25 mm, there was an initial decrease in specific power, followed by an improved with rising rotation speed. Under the other diameters of droplets studied, the specific power showed a monotonic decline with increasing rotation speed. Specific power remained constant when the rise in volume efficiency equaled the increase in consumption of power. However, there was an increase in specific power when the former was lower than the latter.

At a fixed rotation speed, specific power increased with increasing diameter of droplets. At a high rotation speed, the increase in diameter of droplet resulted in a greater increase in specific power compared to that at a low rotation speed. Increase in the diameter of droplets from 0.15 mm to 0.25 mm caused a rise in specific power 0.49 kW/(m^3/min) at 3000 rpm, and 0.17 kW/(m^3/min) at 1500 rpm.

4. Conclusions

The current study developed a thermodynamics theoretical

model of a WLSSAC to identify the impacts of rotation speed, discharge pressure, water injection flow rate and diameter of droplets on the performance of the compressor. The following conclusions were made:

1) Increasing the rate of water injection reduced the temperature of discharge, resulted in the compression procedure transitioning to isothermal compression, and improved compressor performance. Under rated conditions, the rate of water injection increased from 60 L/min to 80 L/min, the discharge temperature of the compressor decreased from 320.6 K to 309.5 K, the volume efficiency increased from 78.9 % to 80.4 %, and the adiabatic efficiency increased from 72.2 % to 75.0 %.

2) The increase in rotation speed reduced leakage duration and thus leakage quantity, which improved the efficiency of the compressor. At the same time, heat transfer and sealing performance were affected due to the decline in the water-gas volume ratio, resulting in a reduction in the efficiency of the compressor. When the impact of the latter exceeded that of the former, the efficiency of the compressor decreased with increasing rotation speed.

3) Water injection atomization increased the heat transfer area between water and humid air and improved the compressor performance.

4) To guarantee the high performance of the compressor, the water-gas volume ratio should be guaranteed within the range of 2 %-3 %, which is very different to the equivalent ratio of the oil-injected single-screw air compressor. At the same time, the compressor should be operated under rated working conditions as far as possible. Water injection atomization treatment can be considered to ensure the impact of water injection atomization.

Acknowledgments

The authors gratefully acknowledge research funding provided by the Beijing Municipal Natural Science Foundation (No. 3181001).

Nomenclature

C : Flow coefficient
c : Specific heat, J/(kg·K)
c_r : Correction coefficient of helically coiled tube
d : Diameter, mm; Humidity ratio of humid air
f : Slip factor
h : Specific enthalpy, J/kg
k : Heat convection coefficient, W/(m^2·K)
L : Length, m
m : Mass of fluid, kg
Nu : Nusselt number
n : Rotation speed of screw rotor, rpm
P : Power, W
Pr : Prandlt number
p : Pressure, Pa
Q : Heat transfer quantity, J
Re : Reynolds number
r_1 : Radius of the screw rotor, m
r_2 : Radius of the gate rotor, m
r_o : Outside radius of rotor, m
r_i : Inside radius of rotor, m
r_l : Latent heat of water, J/kg
S : Area, m^2
T : Temperature, K
q_v : Volume flow of fluid, m^3/s
u : Specific internal energy, J/kg
V : Volume, m^3
v : Velocity, m/s; Specific volume, m^3/kg
W : Work, J
z : Potential head, m

Greek symbols

α : Void fraction
β : Kinetic energy correction factor
ζ : Atomization rate
θ : Rotation angle of screw rotor, rad
λ : Thermal conductivity, W/(m·K)
μ : Dynamic viscosity, N·s/m^2
ρ : Density, kg/m^3
χ : Mass fraction of gas
ω : Angular velocity of screw rotor

Subscripts

a : Dry air
ad : Adiabatic compression
c : Control volume
d : Discharge
e : Evaporation
g : Gas mixture
in : Inflow of control volume
inj : Water injection
l : Water
lea : Leakage of fluid
out : Outflow of control volume
$real$: Real value
th : Theoretical value
v : Saturated water vapor

References

[1] Y. Y. Zhao, L. S. Li and H. G. Wu, Theoretical and experimental studies of water injection scroll compressor in automotive fuel cell systems, *Energy Conversion and Management*, 46 (9-10) (2005) 1379-1392.

[2] J. F. Li, H. G. Wu and B. M. Wang, Research on the performance of water-injection twin screw compressor, *Applied Thermal Engineering*, 29 (2009) 3401-3408.

[3] J. B. Shen, Z. W. Xing and X. L. Wang, Analysis of a single-effect mechanical vapor compression desalination system us-

ing water injected twin screw compressors, *Desalination*, 333 (2014) 146-153.
[4] C. Wang, Z. W. Xing and W. Q. Chen, Development of an oil free water-lubricated twin-screw air compressor, *Applied Thermal Engineering*, 143 (2018) 396-402.
[5] C. Wang, Z. W. Xing and W. Q. Chen, Analysis of the leakage in a water-lubricated twin-screw air compressor, *Applied Thermal Engineering*, 155 (2019) 217-225.
[6] Y. F. Tian, J. B. Shen and C. Wang, Modeling and performance study of a water-injected twin-screw water vapor compressor, *International Journal of Refrigeration*, 83 (2017) 75-87.
[7] Z. L. Wang, Z. Liu and H. Wang, Geometric characteristics analysis for inner surface of working chamber in single screw compressor with multicolumn envelope meshing pair, *International Journal of Refrigeration*, 108 (2019) 347-357.
[8] Z. L. Wang, H. Wang and Z. M. Wang, Theoretical study on heat transfer characteristics of single screw refrigeration compressor with Multicolumn envelope meshing pair, *Applied Thermal Engineering*, 166 (2020) 114536.
[9] Z. L. Wang, Z. Liu and W. F. Wu, Research of leakage characteristics of single screw refrigeration compressors with the multicolumn envelope meshing pair, *International Journal of Refrigeration,* 49 (2015) 1-10.
[10] Q. Y. Wen, R. P. Zhi and Y. T. Wu, Performance optimization of a heat pump integrated with a single-screw refrigeration compressor with liquid refrigerant injection, *Energy*, 207 (2020) 118197.
[11] Y. W. Lu, S. W. Liu and Y. T. Wu, Performance improvement of single screw compressor by meshing clearance adjustment used in refrigeration system, *Journal of Thermal Science,* 30 (2020) 149-164.
[12] T. Li, W. Jiang and X. T. Gan, A theoretical method for evaluating the lubrication performance of the meshing pair profiles in water flooded single screw compressors based on the micro deflecting motion trajectory, *Applied Sciences*, 10 (2020) 5244.
[13] T. Li, R. Huang and Q. K. Feng, Hydrodynamic lubricating characteristics of water flooded single screw compressors based on two types of meshing pair profile, *Proceedings of the Institution of Mechanical Engineers, Part J: Journal of Engineering Tribology*, 230 (9) (2016) 1092-1106.
[14] T. Li, Z. Liu and R. Huang, Research of the hydrodynamic lubrication characteristics of different meshing pair profiles in water-flooded single screw compressors, *Proceedings of the Institution of Mechanical Engineers, Part A: Journal of Power and Energy*, 230 (3) (2016) 247-259.
[15] T. Li, Y. C. Wang and X. L. Mao, Development and experi mental study of the first stage in a two-stage water-flooded single-screw compressor unit for polyethylene terephthalate bottle blowing system, *Energies*, 13 (2020) 4232.
[16] J. L. Yang, C. Zhang and Z. T. Zhang, Study on mechanical vapor recompression system with wet compression single screw compressor, *Applied Thermal Engineering*, 103 (2016) 205-211.
[17] L. L. Shen, W. Wang and Y. T. Wu, A study of clearance height on the performance of single screw expanders in small-scale organic Rankine cycles, *Energy*, 153 (2018) 45-55.
[18] L. L. Shen, W. Wang and Y. T. Wu, Theoretical and experimental analyses of the internal leakage in single-screw expanders, *International Journal of Refrigeration*, 86 (2018) 273-281.
[19] H. G. Wu, Z. W. Xing and P. C. Shu, Theoretical and experimental study on indicator diagram of twin screw refrigeration compressor, *International Journal of Refrigeration*, 27 (2004) 331-338.
[20] Z. Y. Wu and G. L. Tao, Simulation of high speed single screw compressor in fuel cell, *Journal of Zhejiang University*, 40 (2) (2006) 309-313.
[21] Y. F. Tian, Z. W. Xing and Z. L. He, Modeling and performance analysis of twin-screw steam expander under fluctuating operating conditions in steam pipeline pressure energy recovery applications, *Energy*, 141 (2017) 692-701.
[22] S. M. Yang and W. Q. Tao, *Heat Transfer*, 4th Ed., Higher Education Press, Beijing (2006).
[23] Y. N. Li, J. F. Wang and Y. T. Wu, Influence of water injection atomization on the performance of water-lubricated single-screw air compressor, *2021 2nd International Conference on Energy Power and Automation Engineering* (2021).

Yanan Li got her Master's degree from Yanshan University, China, in 2011. Now she is a Post-graduate student at Beijing University of Technology. Her research interests in water-lubricated single-screw air compressor.